Mon. Not. R. Astron. Soc. **000**, 1–16 (2011) Printed 3 April 2014 (MN LATEX style file v2.2)

Stellar dynamics in gas: The role of gas damping

Nathan W. C. Leigh[1,2], Alessandra Mastrobuono Battisti[3], Hagai B. Perets[3,4], Torsten Böker[5] ⋆

[1] *Department of Physics, University of Alberta, CCIS 4-183, Edmonton, AB T6G 2E1, Canada*
[2] *Department of Astrophysics, American Museum of Natural History, Central Park West and 79th Street, New York, NY 10024*
[3] *Physics Department, Technion: Israel Institute of Technology, Haifa, Israel 32000*
[4] *Deloro Fellow*
[5] *European Space Agency, Space Science Department, Keplerlaan 1, 2200 AG Noordwijk, The Netherlands*

arXiv:1404.0379v1 [astro-ph.SR] 1 Apr 2014

3 April 2014

ABSTRACT

In this paper, we consider how gas damping affects the dynamical evolution of gas-embedded star clusters. Using a simple three-component (i.e. one gas and two stellar components) model, we compare the rates of mass segregation due to two-body relaxation, accretion from the interstellar medium, and gas dynamical friction in both the supersonic and subsonic regimes. Using observational data in the literature, we apply our analytic predictions to two different astrophysical environments, namely galactic nuclei and young open star clusters. Our analytic results are then tested using numerical simulations performed with the NBSymple code, modified by an additional deceleration term to model the damping effects of the gas.

The results of our simulations are in reasonable agreement with our analytic predictions, and demonstrate that gas damping can significantly accelerate the rate of mass segregation. A stable state of approximate energy equilibrium cannot be achieved in our model if gas damping is present, even if Spitzer's Criterion is satisfied. This instability drives the continued dynamical decoupling and subsequent ejection (and/or collisions) of the more massive population. Unlike two-body relaxation, gas damping causes overall cluster contraction, reducing both the core and half-mass radii. If the cluster is mass segregated (and/or the gas density is highest at the cluster centre), the latter contracts faster than the former, accelerating the rate of core collapse.

Key words: open clusters and associations: general – galaxies: nuclei – galaxies: star clusters – stars: formation – stars: black holes – stars: kinematics and dynamics.

1 INTRODUCTION

The advances made in telescope resolution over the last few decades have revealed the properties of a number of interesting astrophysical environments that contain both gas and stars in significant quantities. For example, the properties of many young star-forming regions throughout our Galaxy have now been catalogued using the unprecedented spatial resolution of the Hubble Space Telescope (HST), and large ground-based telescopes assisted by adaptive optics (e.g. Wang et al. 2011; Phan-Bao et al. 2011; De Marchi, Panagia & Sabbi 2011; Da Rio et al. 2012). The gas being used to form stars in these regions is typically dense and cold, with densities and temperatures on the order of $\sim 10^2 - 10^6$ $M_\odot$ pc^{-3} and ~ 10 K (temperatures can reach ~ 30 K during the later stages of star formation) (e.g. Lada & Lada 2003; McKee & Ostriker 2007), respectively. The nuclei of spiral galaxies have also been imaged at high resolution, revealing not only that significant quantities of molecular gas are present, but also that star formation is on-going in these dense stellar environments (e.g. Böker, Lisenfeld & Schinnerer 2003; Schinnerer et al. 2006). The implications of the presence of gas in galactic nuclei, both with respect to the formation of nuclear star clusters and the growth of super-massive black holes (SMBHs) are not yet fully understood (e.g. Hopkins & Quataert 2011; Gabor & Bournaud 2013; Kormendy & Ho 2013). Additionally, recent evidence suggests that globular clusters (GCs) underwent prolonged star formation early on in their lifetimes (see Gratton, Carretta & Bragaglia (2012) for a recent review). That is, gas was present in significant quantities for the first $\sim 10^8$ years, albeit perhaps intermittently (Conroy & Spergel 2011; Conroy 2012). This evidence

⋆ E-mail: nleigh@ualberta.ca (NL), alessandra.mastrobuono@gmail.com (AM), hperets@ph.technion.ac.il (HP), tboeker@rssd.esa.int (TB)

© 2011 RAS

comes in the form of multiple stellar populations identified in the colour-magnitude diagram (e.g. Piotto et al. 2007), as well as curious abundance anomalies that cannot be explained by a single burst of star formation (e.g. Osborn 1971; Gratton et al. 2001). Thus, at least until the second generation has formed, stars from the first generation must have been orbiting within a gas-rich environment.

On the theoretical front, most studies conducted to date considered one of two extremes. The first has its focus purely on the stellar dynamics (see Spitzer (1987) and Heggie & Hut (2003) for detailed reviews), long after the gas has been converted to stars and/or ejected from the cluster. The focus of the second extreme is often on the very early stages of star formation (e.g. Krumholz, McKee & Klein 2005b; Kirk & Myers 2011; Krumholz, Klein & McKee 2011; Krumholz 2011; Offner & McKee 2011; Krumholz, Klein & McKee 2012; Kirk, Offner & Redmond 2014), when gas is first being converted into stars. Little theoretical work has been done connecting these two extremes, when both gas and stars co-exist in significant quantities, particularly in massive clusters and for more than a few tens of Myr.

Bonnell et al. (1997) first studied gas accretion onto small clusters of young stars using a three-dimensional SPH code. The authors find that non-uniform or differential accretion can produce a realistic mass spectrum, even when the initial stellar masses are uniform, and tends to form massive stars at the cluster centre where the gas density is highest (e.g. Bonnell & Davies 1998; Bonnell et al. 2001). Later, Bate, Bonnell & Bromm (2003) performed a larger numerical simulation to resolve the fragmentation process down to the opacity limit. The authors find that the star formation process is highly chaotic and dynamic, and that the observed statistical properties of stars are a natural consequence of a dynamical environment. These results were later expanded upon by Bate (2009), Bate (2012) and Maschberger et al. (2010) to include more massive clusters composed of $\sim$ a few thousand stars. Other authors placed their focus on the evolving properties of the gas (Offner, Hansen & Krumholz 2009), the impact of different initial conditions (Girichidis et al. 2012a) or the evolution of potential and kinetic energy throughout the cloud (Girichidis et al. 2012b), and showed that clusters tend to be born in a subvirial state (e.g. Allison et al. 2009b). Both the gas velocity dispersion and temperature can be surprisingly high, especially if radiative feedback is included in the simulations (e.g. Offner, Hansen & Krumholz 2009; Offner et al. 2009). Along with large-scale magnetic fields (e.g. Lee et al. 2014), this can dramatically reduce not only the overall accretion rate, but also the final number of stars that form. A number of N-body simulations have also been performed to study the effects of gas expulsion or dispersal (e.g. Marks, Kroupa & Baumgardt 2008; Moeckel et al. 2012), sub-cluster merging (e.g. Moeckel & Bonnell 2009b), primordial mass segregation (e.g. Marks, Kroupa & Baumgardt 2008; Moeckel & Bonnell 2009a), and even techniques to quantify the degree of mass segregation (Allison et al. 2009a; Parker & Meyer 2012; Parker et al. 2014).

In purely stellar systems (i.e. gas-free), two-body relaxation is the dominant physical mechanism driving the evolution of star clusters for most of their lifetime (e.g. Henon 1960, 1973; Spitzer 1987; Heggie & Hut 2003; Gieles, Heggie & Zhao 2011). Long-range gravitational interactions tend to push the cluster toward a state of energy equipartition in which all objects have comparable kinetic energies.[1] Consequently, the velocities of the most massive objects decrease, and they accumulate in the central regions of the cluster. Similarly, the velocities of the lowest mass objects increase, and they are subsequently dispersed to wider orbits. This mechanism is called mass segregation, and has been observed in both young and old clusters (e.g. Lada & Lada 2003; von Hippel & Sarajedini 1998; De Marchi, Paresce & Portegies Zwart 2010).

In the presence of gas, other effects could also contribute to the deceleration of a massive test particle. For example, mass accretion reduces the accretor velocity due to conservation of momentum. This was first argued by Bondi & Hoyle (1944) and Bondi (1952) in the supersonic and subsonic limits, respectively. Several authors have also explored the effects of gas dynamical friction, particularly in the steady-state supersonic regime (e.g. Dokuchaev 1964; Ruderman & Spiegel 1971; Rephaeli & Salpeter 1980; Ostriker 1999), although it is most effective when the perturber velocity is approximately equal to the sound speed of the surrounding gaseous medium. More recently, Lee & Stahler (2011) and Lee & Stahler (2013) showed that the drag force should be precisely equal to $\dot{m}$v, where $\dot{m}$ is the rate of mass accretion and v is the accretor's velocity relative to the gas, in both the subsonic and supersonic regimes. Consequently, the authors argued that damping due to gas dynamical friction cannot be separated from that due to accretion, and that these processes instead represent different components of the same underlying damping mechanism.

In this paper, we address the question: When does the presence of gas in a stellar system significantly affect the stars' dynamics? To answer this question, we will adopt a three-component model to calculate and compare three timescales for a massive test particle orbiting within the cluster potential to become mass segregated. The damping mechanisms we consider are two-body relaxation, accretion from the interstellar medium (ISM) and gas dynamical friction. To first order, this will allow us to constrain the parameter space in the cluster mass-gas density plane for which each of the different damping mechanisms dominates the deceleration of the test particle. We then apply our results to observed data taken from the literature for two different types of astrophysical environments, namely the galactic nuclei of late-type spirals and young star-forming regions, and determine the dominant damping mechanism operating in each.

We compare all three timescales in both the subsonic and supersonic regimes in Section 2, and apply our analytic model to the available observational data. The modified N-body simulations used to model the effects of gas damping are presented in Section 3, and compared to the predictions of our analytic model, the details of which are provided in an Appendix. Finally, in Section 4, we summarize our key results, and discuss the significance of our results for differ-

[1] In reality, such an idealized state is never fully achieved in a cluster with a realistic mass spectrum or potential; see Trenti & van der Marel (2013) for more details.

ent astrophysical environments, in particular galactic nuclei and young star-forming regions.

2 ANALYTIC MODEL

In this section, we present the results of our analytic model, the details of which are presented in Appendix A, along with a discussion of our model assumptions. Using our model, we derive the approximate time for a massive test particle to become mass segregated – i.e. reach an orbit within the cluster that is approximately consistent with energy equipartition or, more accurately, energy equilibrium (Trenti & van der Marel 2013) – in a spherical, self-gravitating, pressure-supported, stellar system embedded in a gaseous medium. This is done by evaluating the deceleration induced on the particle by, and hence the timescale for, each of the relevant damping mechanisms to reduce the speed of the test particle from σ to $\sigma\sqrt{\bar{m}/m_1}$, where σ is the root-mean-square velocity, $\bar{m}$ is the average particle mass and m_1 is the mass of the test particle. To first-order, we ignore the shape of the gravitational potential, and assume that gas damping will act to smoothly decrease the root-mean-square speeds of the stars over time.[2] The damping mechanisms we consider are two-body relaxation, gas dynamical friction and accretion from the ISM. Using our analytic timescales, we further solve for the parameter space in the cluster mass-gas density plane for which each of these mechanisms dominates the deceleration of a massive test particle.

In principle, our analytic model is suitable to a number of astrophysical scenarios, including a massive star orbiting within a gas-embedded star cluster, a primordial globular cluster orbiting within the natal Milky Way, or even galaxies orbiting within galaxy clusters. For the remainder of this paper, however, we present our model within the context of a gas-embedded star cluster in order to keep the discussion as simple and direct as possible, and to facilitate comparisons to the rich body of observational data and theoretical models for resolved star clusters available in the literature.[3] The results of our model are applied to different astrophysical environments for which the relevant observational measurements are available in the literature, specifically young star-forming regions and galactic nuclei.

2.1 Timescales

We show in Figure 1 the timescales for gas dynamical friction and two-body relaxation as a function of the total stellar mass (the mass in gas is not included on the x-axis) for both the subsonic (left panel) and supersonic (right panel) cases. We adopt $r_h = 20$ pc, and do not plot the timescale for accretion to avoid over-populating Figure 1. Instead, we show the cumulative timescale, calculated from the sum of the rates of all three damping mechanisms (i.e. including accretion). Recall that, for a given test particle mass, the timescale for accretion to operate is directly proportional to the timescale for gas dynamical friction.

In the subsonic case, shown in the left panel of Figure 1, the timescale required for gas accretion to operate is always longer than the gas dynamical friction (blue lines) timescale by a factor ~ 2.5. However, both timescales are considerably shorter than the corresponding two-body relaxation time at high gas densities. Specifically, at a gas density 10^3 cm^{-3} (shown by the solid lines in Figure 1) two-body relaxation dominates over gas dynamical friction provided the total stellar mass $\lesssim 10^{7.7}$ M$_\odot$. At higher gas densities (shown by the short- and long-dashed lines in Figure 1), gas dynamical friction always dominates the rate of mass segregation, and two-body relaxation always plays a negligible role independent of the total stellar mass.

In the supersonic case, shown in the right panel of Figure 1, the timescale for gas dynamical friction (blue lines) to operate is always shorter than the accretion timescale (not shown in Figure 1) by a factor ~ 10. The gas dynamical friction timescale tends to be shorter than the two-body relaxation timescale (red lines) for low total stellar masses, but becomes longer than the two-body relaxation timescale for high total stellar mass. This transition shifts to higher total stellar masses as the gas density increases. We note as well that for larger r_h, gas dynamical friction and accretion can dominate over two-body relaxation at lower gas densities, but assuming a fixed total stellar mass. The perhaps counter-intuitive result that the two-body relaxation timescale is *shorter* than the timescales for gas accretion and gas dynamical friction at large total cluster masses can be understood as follows. The timescales for both accretion and gas dynamical friction scale as v^3, where v is the velocity of the test particle with respect to the gas. A higher gas density implies a higher total gas mass, which translates into higher stellar velocities via the virial theorem.

2.2 Identifying the dominant damping mechanism

Next, we show in Figure 2, for both the subsonic (left panel) and supersonic (right panel) cases, the parameter space in the cluster mass-gas density plane for which each of the different damping mechanisms dominates the rate of deceleration of a massive test particle. The regions dominated by two-body relaxation and gas dynamical friction are indicated by "TBR" and "GDF", respectively. The solid and dashed lines in Figure 2 correspond to the relations between the total (gas and stars) cluster mass and average gas density obtained by equating each combination of the derived timescales. These relations are $\tau_{\rm df} = \tau_{\rm rh}$ (solid lines) and $\tau_{\rm acc} = \tau_{\rm rh}$ (dashed lines). These lines divide the parameter space for which gas dynamical friction and accretion each dominate over two-body relaxation. We exclude the relation $\tau_{\rm df} = \tau_{\rm acc}$ since, as shown in the previous section, the rate of deceleration due to gas dynamical friction is always greater than the rate for gas accretion. The dotted lines show the cluster mass-gas density relations for constant gas mass fractions $\alpha = M_g/M_s$.

[2] As we will show, the final velocity plays a negligible role in deciding the mass segregation times due to gas dynamical friction and accretion.

[3] Note that, since we focus on the star cluster case in this paper, we do not consider stellar dynamical friction, which is more appropriate for larger systems where the assumption is valid that the massive body undergoing stellar dynamical friction moves in an infinite sea of low-mass particles.

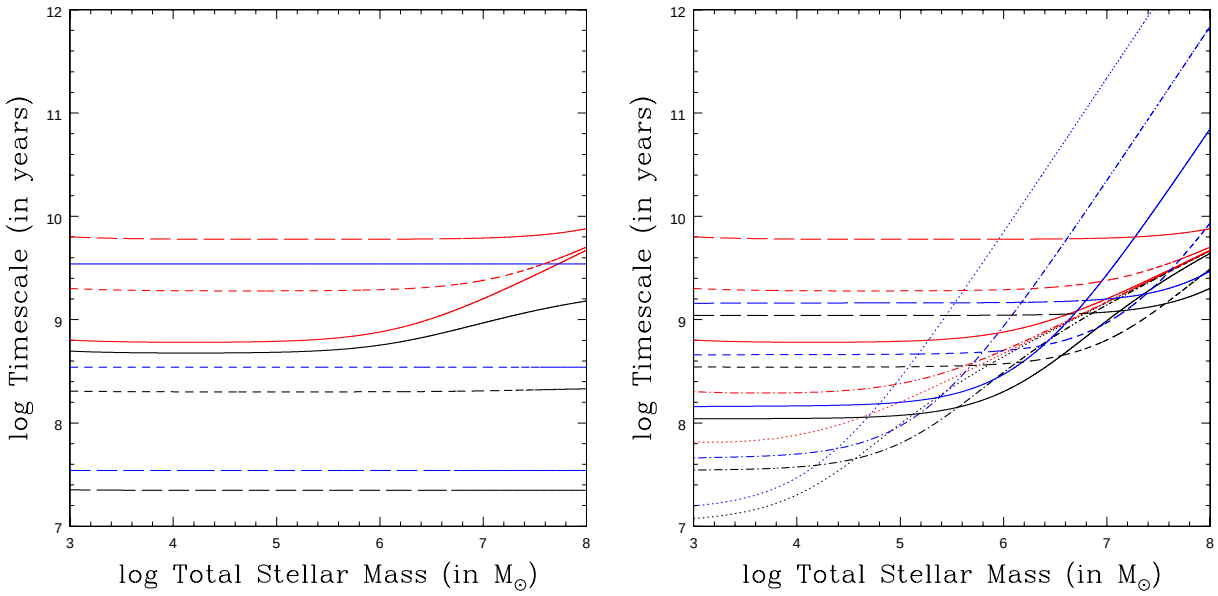

Figure 1. Timescales for two-body relaxation and gas dynamical friction are shown as a function of the total stellar mass assuming subsonic motion with $c_s = 10$ km/s (left panel), or supersonic motion with $c_s = 0.1$ km/s (right panel). The mass of the test particle is taken to be 32.55 $M_\odot$. The red lines correspond to the two-body relaxation timescales, the blue lines to the gas dynamical friction timescales, and the black lines to the cumulative or total timescales calculated from the sum of the rates of all three mechanisms. The dotted, dash-dotted, solid, short-dashed, and long-dashed lines correspond to average gas densities of 10 cm^{-3}, 10^2 cm^{-3}, 10^3 cm^{-3}, 10^4 cm^{-3} and 10^5 cm^{-3}, respectively.

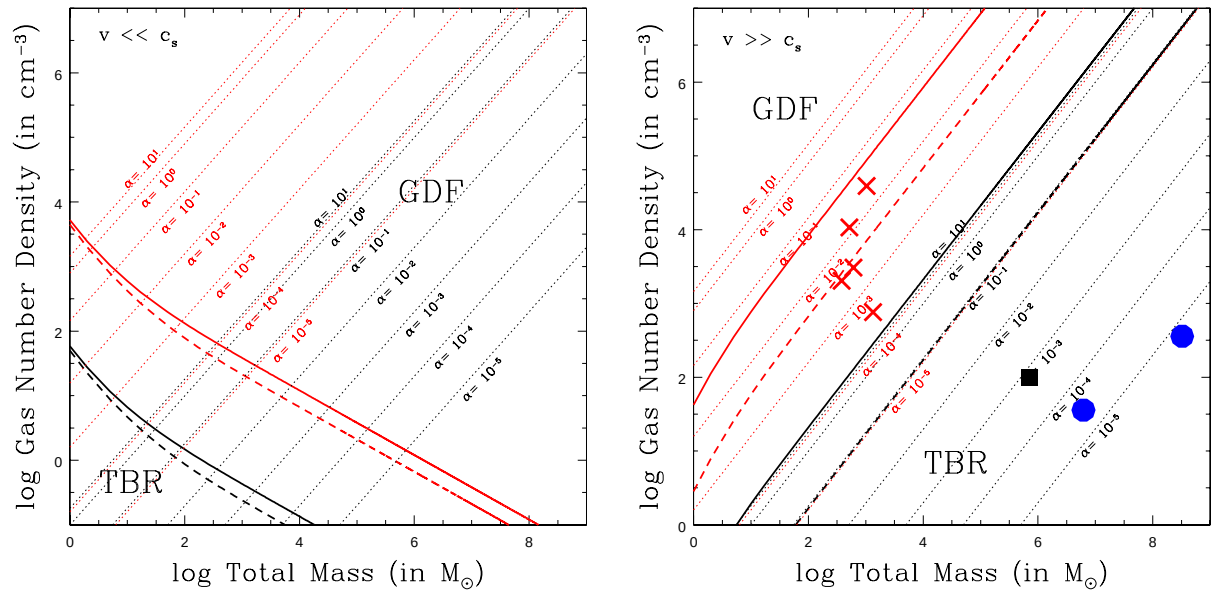

Figure 2. The parameter space in the cluster mass-gas density-plane for which each damping mechanism dominates the deceleration of a massive test particle. This is shown for both subsonic (left panel) and supersonic (right panel) motion. The regions dominated by two-body relaxation and gas dynamical friction are indicated by "TBR" and "GDF", respectively. The total cluster mass, shown on the x-axis, is calculated as the sum of the total mass in gas and stars. The mass of the test particle is taken to be 32.55 $M_\odot$. The black lines adopt a half-mass radius for the cluster of $r_h = 20$ pc, whereas the red lines adopt $r_h = 1$ pc. The solid lines correspond to $\tau_{rh} = \tau_{acc}$, and the long-dashed lines to $\tau_{rh} = \tau_{df}$. The dotted lines correspond to constant gas mass fractions $\alpha = M_g/M_s$. The blue circles correspond to the nuclei of the late-type spiral galaxies NGC 6946 (Schinnerer et al. 2006) and IC 342 (Schinnerer, Böker & Meier 2003). The black square is the Milky Way Galactic Centre (Launhardt, Zylka & Mezger 2002). The red crosses correspond to observed data taken from Lada & Lada (2003) for young open clusters or associations.

2.2.1 Subsonic

As shown in the left panel of Figure 2, two-body relaxation can dominate at low total cluster masses in the subsonic regime, provided the gas density is also low. At sufficiently large total cluster masses, however, gas damping dominates over two-body relaxation independent of the gas density. For instance, for a total cluster mass $\sim 10^6$ $M_\odot$ and half-mass radius $r_h = 1$ pc, gas damping dominates for all gas densities. If the half-mass radius r_h increases, the lines shift to a lower gas density at fixed cluster mass, and the distance between the lines increases slightly, with increasing particle mass.

2.2.2 Supersonic

In the supersonic regime, very high gas densities are needed in massive clusters for accretion and gas dynamical friction to supersede two-body relaxation as the dominant damping mechanism. This is illustrated in the right panel of Figure 2 by the positive slope of the lines. For large cluster masses and low gas densities (i.e. for small gas mass fractions), two-body relaxation dominates over both accretion and gas dynamical friction. At low cluster masses, both accretion and gas dynamical friction dominate independent of the gas density, provided $r_h \gtrsim 15$ pc. As r_h decreases, the y-intercept of the lines shifts to higher gas densities at fixed cluster mass. Both the slopes and y-intercepts of the lines are roughly insensitive to our choice for the mass of the test particle.

2.3 Application to observational data

In order to apply our results to observed gas-rich clusters, we take data from the literature to obtain total cluster masses and average gas densities. This is done for two different types of astrophysical environments, namely galactic nuclei and young star-forming regions. Specifically, we apply our model to the galactic nuclei of the Milky Way (black squares in Figure 2), NGC 6946 and IC 342 (blue circles) (Launhardt, Zylka & Mezger 2002; Schinnerer et al. 2006; Schinnerer, Böker & Meier 2003), as well as to the young star-forming regions Mon R2, NGC 1333, NGC 2024, NGC 2068, NGC 2071 (red crosses) (Lada & Lada 2003). The observed data for these nuclear and open clusters are provided in Table 1, and the results of applying our model to these data are shown in Figure 2. The location of each point in the mass-density-plane tells us which damping mechanism is currently dominating in that environment. *In order to see this, the red crosses should be compared to the red lines, and the black squares and blue circle should be compared to the black lines.* We include the observed data points only in the right panel of Figure 2 since, as we explain below, we expect the stellar motions to be in the supersonic regime in all environments considered here.

The gas in the inner 1.25 pc of the Galactic Centre is hot and ionized. However, we still expect the stellar motions to most likely be in the supersonic regime due to the large stellar velocities. This may also be the case for IC 342, which is thought to be similar to the Milky Way Galactic Centre. The right panel of Figure 2 suggests that two-body relaxation dominates in these environments if the motion is supersonic. Even if the stars are in the subsonic regime, the left panel of Figure 2 suggests that two-body relaxation should still dominate in these regions. Importantly, this remains the case if the black lines in Figure 2 are shifted to correspond directly to the observed half-mass radii for these nuclear star clusters, both in the supersonic and subsonic regimes.

The gas in the remaining environments shown in Table 1 is predominantly molecular hydrogen. Hence, we expect the stellar motions to be mainly supersonic. In this regime, the right panel of Figure 2 suggests that two-body relaxation dominates in all but two young open clusters. These are NGC 1333 and NGC 2071, which have the highest gas densities. Importantly, however, our model adopts $r_h = 1$ pc for the red lines, which is slightly too large for these two low-mass open clusters (see Table 1). For smaller r_h, the y-intercepts of the lines in Figure 2 shift upward to higher gas densities. For NGC 1333 and NGC 2071, the end result is that the rates of mass segregation due to two-body relaxation and gas dynamical friction are roughly equal. Thus, we conclude that for the open clusters considered here, the rate of mass segregation due to two-body relaxation tends to be comparable to, but slightly exceeds, the rates from gas dynamical friction and accretion.

3 COMPUTATIONAL MODELS

In this section, we present and discuss the results of our computational N-body simulations modified to include the effects of gas damping (but not the gas potential itself).

3.1 The models

We wish to test the analytic theory presented in the previous section. This is done to evaluate the effects of gas damping on the overall cluster evolution, and the degree to which gas damping can accelerate the rate of mass segregation - i.e. the rate at which the most massive members in a self-gravitating system end up at the bottom of the potential well. To do this, we use computational N-body models for star cluster evolution performed using an adapted version of the NBSymple code (Capuzzo-Dolcetta, Mastrobuono-Battisti & Maschietti 2011) to simulate mass segregation in a gas-embedded star cluster. We consider only the steady-state supersonic limit in our simulations, since the gas in most astrophysical cases of interest is typically cold and molecular, with a correspondingly low sound speed.

To model the effects of the gas, we introduce an additional deceleration on each N-body particle equal to that due to gas dynamical friction, given in Equation A13. This is used to reduce the velocity of every N-body particle at each time-step. We consider only the deceleration induced by gas dynamical friction in our computational models, since a quick comparison of the timescales derived in the preceding section reveals that gas dynamical friction is more effective than gas accretion in the supersonic regime (for the range of particle velocities and masses considered here). We note that, neglecting the dependence on the test particle mass, the timescales for accretion and gas dynamical friction are

Table 1. Observational parameters for each cluster/nucleus

Cluster/Nucleus	log Total Mass[a] (in $M_\odot$)	log Gas Density (in cm^{-3})	Size (in pc)
Mon R2[b]	3.13	2.88	1.85
NGC 1333	3.01	4.59	0.49
NGC 2024	2.79	3.49	0.88
NGC 2068	2.58	3.31	0.86
NGC 2071	2.71	4.03	0.59
IC 342[c]	6.79	1.55	30.00
NGC 6946[d]	8.51	2.55	60.00
MW[e]	5.85	2.00	1.25

[a]Including both the stellar and gas mass.
[b]All open cluster data is taken from Lada & Lada (2003).
[c]Data for the late-type spiral galaxy NGC 6946 is taken from (Schinnerer et al. 2006), and 30 pc is the limiting radius considered in the study.
[d]Data for the late-type spiral galaxy IC 342 is taken from (Schinnerer, Böker & Meier 2003), and 60 pc is the limiting radius considered in the study.
[e]Data for the Milky Way Galactic Centre is taken from (Launhardt, Zylka & Mezger 2002) and Merritt (2013), and corresponds only to the inner 1.25 pc.

equivalent to within a dimensionless constant, given by the ratio between Equation A12 and Equation A19. Thus, our chosen form for the deceleration on a massive test particle is representative of gas damping in general to within a dimensionless constant.

For all models, we assume a gas composed entirely of hydrogen molecules (i.e. $m_3 = 3.3 \times 10^{-27}$ kg), with a gas density $n = 4 \times 10^3$ cm^{-3}. The sound speed is chosen to be very low $c_s \ll \sigma$ to ensure that the motion is always in the steady-state supersonic regime. This means that our chosen form for the deceleration induced by gas damping given in Equation A13 is always applicable. All models assume stellar masses $m_1 = 32.55$ $M_\odot$ and $m_2 = 3.255$ $M_\odot$. These masses are chosen to yield the desired total cluster masses for our simulations (see below), however they are in general representative of stellar masses observed in young massive star-forming regions. Stellar evolution does not occur in any of our simulations, so that the stellar masses are time-independent.

We consider two different cases. Case 1 adheres to Spitzer's Criterion, with the total mass in species 1 being much less than the total mass in species 2. If Spitzer's Criterion is satisfied, then a stable state of energy equilibrium (e.g. energy equipartition) should be achievable between both mass species. If not, the heavier species decouples dynamically from the lighter species, interacting primarily with other members of the heavier species in the central cluster regions. Case 1 is tailored for comparison to our analytic model. Case 2 assumes that the total number of stars is split equally between the two mass-components. In this case, we do not compare our analytic calculations to the results of our simulations, since this deviates from the assumptions of our analytic model. Dividing the total number of stars equally between both mass species allows us to construct meaningful surface density profiles for each of them individually. This facilitates quantifying the effects of gas accretion and gas dynamical friction on the overall cluster structure. We also follow the evolution of the cluster considered in Case 2 to core collapse.

For Case 1, the total number of stars belonging to species 1 and 2 are, respectively, $N_1 = 100$ and $N_2 = 15260$. This gives a total cluster mass 5.29×10^4 $M_\odot$, and an average stellar mass of $\bar{m} = 3.45$ $M_\odot$. The initial half-mass radius is 3.9 pc before the cluster experiences an intial phase of expansion, after which it is 6.1 pc (at t = 3 Myr). The cluster orbits within the Galactic potential on a mildly eccentric orbit with e = 0.05, and a distance at perigalacticon of 9.7 kpc. From Equation A4, the initial two-body relaxation time is 1.8×10^8 years.

For Case 2, the total cluster mass 2.75×10^5 $M_\odot$ and the total number of stars is $N_s = 15360$, giving an average stellar mass $\bar{m} = 17.9$ $M_\odot$. The initial core and half-mass radii are 2 pc and 4.05 pc, respectively, and the cluster is modeled assuming a King profile with $W_0 = 5$, initially. The cluster orbits within the Galactic potential assuming the same orbit as in Odenkirchen et al. (2003). From Equation A4, the initial half-mass relaxation timescale is 4.1×10^7 years.

3.2 Comparison to analytic predictions

We begin by comparing the results of our simulations to the predictions of our analytic model, which predicts the time at which the heavier species reaches a mean-square speed $\sim \sigma\sqrt{\bar{m}/m_1}$ from an initial mean-square speed σ. For our models, this implies that the mean-square speed of the heavier species (species 1) must fall by a factor ~ 3 (i.e. from ~ 3.8 kms^{-1} to ~ 1.3 kms^{-1}). Figure 3 shows the time evolution of the root-mean-square speeds of both the light (filled triangles) and heavy (open circles) species, both with (bottom inset) and without (top inset) gas damping. Initially, the clusters expand in our simulations, undergoing an episode of mild violent relaxation.[4] This phase ends at t $\sim$ 3 Myr, at which point steady-state is achieved, and the

[4] This episode of violent relaxation is not accounted for in our analytic model. The initial conditions of our model are only met after this phase of evolution ceases.

system begins to evolve toward a state of energy equilibrium. This corresponds to t = 0 in our analytic model.

The onset of energy equilibrium is depicted in Figure 3, since the root-mean-square speed of the heavier species begins to fall below that of the lighter species. We observe significantly more scatter in the time evolution of the root-mean-square speed of the heavier species, particularly when gas damping is present. This is due mainly to the small number of particles for species 1, but also in part due to strong gravitational interactions that occur between members of species 1 upon segregating into the core. Due to this scatter, the exact time at which energy equilibrium and mass segregation occur is ambiguous in Figure 3. Even more problematic, members of species 1 quickly segregate into the core where the velocity dispersion is at its highest, and this also contributes to increasing the mass in the core, which further increases the central velocity dispersion. Hence, exact energy *equipartition* does not occur in the simulations without gas damping, since the root-mean-square speed of the heavier species never drops as much as energy equipartition initially predicts. Specifically, the root-mean-square speed of the heavier species only falls by at most a factor ~ 1.5 relative to the lighter species after several tens of Myr, at which point the system stabilizes and energy *equilibrium* is reached. This is less than predicted by energy equipartition, as discussed in more detail in Trenti & van der Marel (2013). Only with gas damping does the root-mean-square speed of the heavier species continue to fall below that of the lighter species beyond what is done by two-body relaxation alone. Regardless, it is clear from Figure 3 that gas damping accelerates the rate at which energy equilibrium, and hence mass segregation, occurs by a factor ~ 2 relative to two-body relaxation alone for the model assumptions adopted here.

The predictions of our analytic model are *qualitatively* borne out by the simulations, since gas damping accelerates the rate of mass segregation. Quantitatively, however, our analytic estimates for the mass segregation timescales under-predict the true timescales by a factor $\sim 5-10$, both without and especially with gas damping. Specifically, from Equation A19, mass segregation should begin occurring after 1.2 Myr if only gas dynamical friction is operating (shown by the dashed lines in Figure 3), whereas the half-mass two-body relaxation time (solid lines) for species 1 is 18 Myr, as given by Equation A3 (and ignoring the mass in gas, which is not accounted for in our computational models). Although some members of species 1 do indeed begin to segregate into the core in as a little as a few Myr, the process continues for another few tens of Myr before most members of species are in the core. Thus, our analytic timescales correspond better to the *onset* of mass segregation, as opposed to its termination. Other contributing factors to the discrepany between our analytic timescale and the results of our simulations include the steep dependence of the efficiency of gas damping on the particle velocity, and our adopted estimate of the velocity dispersion (using the approximation in Binney & Tremaine (1987)) which is a slight underestimate for members of species 1 throughout the course of our simulations.

Figure 4 shows snapshots in time of the distribution of stellar velocities for the low- (top insets) and high-mass (bottom insets) species, both with (right insets) and without (left insets) gas damping. The velocities are shown at t = 0 Myr (black) and t = 500 Myr (red). The cluster is on a mildly eccentric orbit, with apogalacticon and perigalacticon speeds of ~ 205 and 230 km/s, respectively. This accounts for most of the offset between the black and red distributions, since the latter corresponds roughly to apogalacticon and the former to shortly after perigalacticon. The smaller peaks at ~ 205 km/s and 215 km/s correspond to tidal tails, which contain approximately half the initial total cluster mass.

Interestingly, in the simulations with gas damping, the cluster is unable to remain in equilibrium, and the heavier species reaches a sufficiently high central density to decouple dynamically from the lighter species. This leads to strong gravitational interactions between members of the heavier species, and ultimately their continual ejection from the cluster over time. With gas damping, a large fraction of species 1 has been ejected from the cluster within < 500 Myr, whereas no members of species 1 have been ejected in the simulation without gas damping. This illustrates that gas damping can significantly accelerate the dynamical ejection of a massive sub-population in clusters, or even stimulate such a population to decouple dynamically and undergo this phase of ejections when it otherwise would remain stable.

This last point is further illustrated in Figure 5, which shows the cumulative radial density profiles for the high- (left insets) and low-mass (right insets) species, both with (top insets) and without (bottom insets) gas dynamical friction. For the high-mass species, the bottom left inset shows that mass segregation has occurred in $\ll 100$ Myr, with all members of species 1 being confined to the central cluster regions. This configuration remains stable in the case without gas damping for the next 500 Myr. With gas damping, however, the heavier species decouples dynamically in $\ll 100$ Myr, and strong gravitational interactions between members of species 1 have ejected a large fraction of the heavier population to large cluster radii, albeit many remain on bound orbits and return to the core within a few Myr. This process of evaporation through strong encounters (Henon 1969) results in the complete ejection of $\gtrsim 80\%$ of the heavier population by 500 Myr.

Approximately half the cluster mass begins to form tidal tails well within 100 Myr, as shown in the cumulative radial density profiles for the lighter species in Figure 5. This is because the cluster is initially tidally over-filling. Note that the evolution is significantly more rapid in the simulations with gas damping.

Next, we present the results of our simulations for which the initial population size of each species is half the total number of objects (i.e. Case 2). This is shown in Figures 6 for the supersonic case, which illustrates the cumulative radial density profiles for the high- (top insets) and low-mass (bottom insets) species, both with (top insets) and without (bottom insets) gas dynamical friction, at 0 Myr (solid lines), 100 Myr (dotted lines) and 500 Myr (dashed lines).

The key result illustrated in Figure 6 is that gas damping causes clusters to contract and compactify, losing stars from their outskirts to tidal tails at an accelerated rate. The stronger is the gas damping, the more pronounced is the effect. This is shown by comparing the cumulative radial density profiles of the heavier (top left inset) and lighter (top right inset) species in the simulations with gas damp-

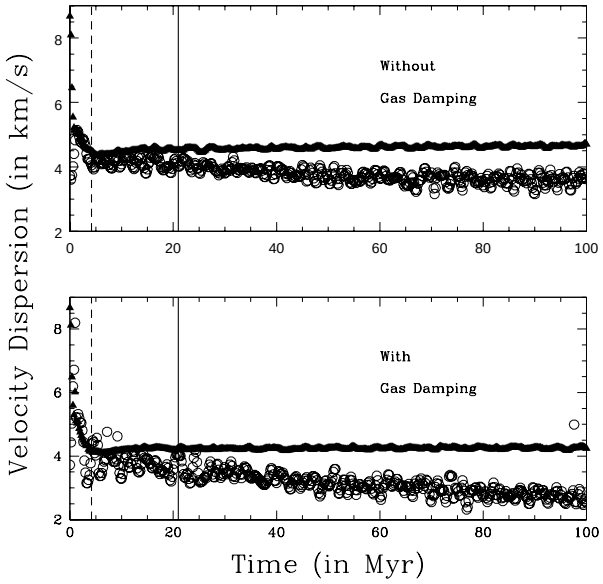

Figure 3. The time evolution of the root-mean-square speeds for the low- (filled triangles) and high-mass (open circles) species are shown, both with (bottom inset) and without (top inset) gas damping. Only stars within 5 pc of the cluster centre are included in calculating the root-mean-square speeds, to avoid including stars that are ejected from the cluster. The dashed and solid lines show our analytic predictions for the timescale for mass segregation due to gas dynamical friction and two-body relaxation, respectively, beginning at t = 3 Myr, which corresponds roughly to the time at which the initial episode of mild violent relaxation ceases, and hence t = 0 in our analytic model.

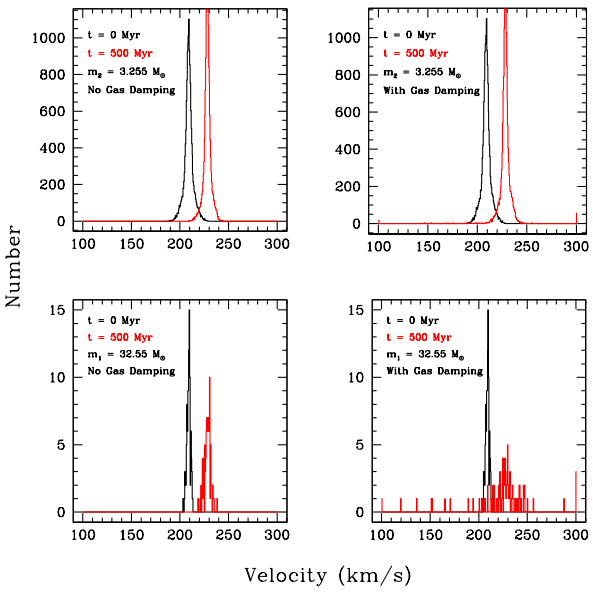

Figure 4. The distribution of stellar velocities are shown for the low- (top insets) and high-mass (bottom insets) species, both with (right insets) and without (left insets) gas damping. The velocities are shown at t = 0 Myr (black) and t = 500 Myr (red).

ing. The lighter species takes considerably longer to undergo this contraction, and even expands on a shorter timescale in response to the loss of cluster mass (of the heavier species). The heavier species, on the other hand, contracts on a much shorter timescale than the lighter species, since the deceleration due to gas damping is proportional to the square of the particle mass.

4 DISCUSSION

In the subsequent sections, we discuss the implications of our results for the evolution of gas-embedded star clusters, comment on the validity of our model assumptions and offer suggestions for improvements in future work. We further discuss what our results imply for different astrophysical cases of interest, including nuclear star clusters and SMBH for-

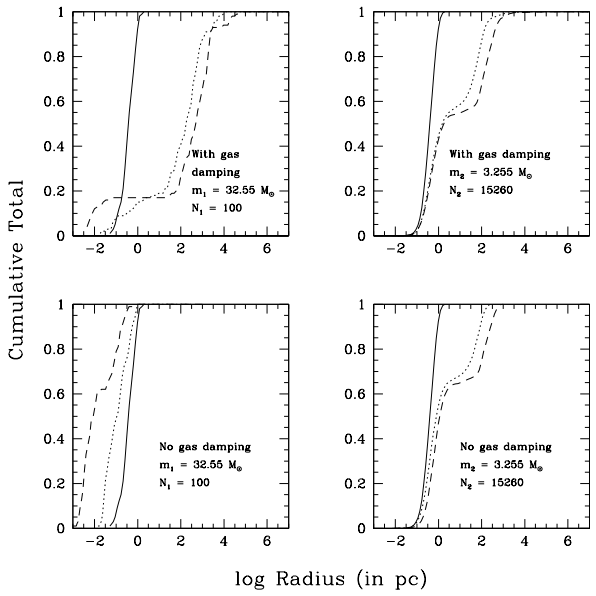

Figure 5. The cumulative radial density profiles are shown for the low- (bottom insets) and high-mass (top insets) species, both with (left insets) and without (right insets) gas damping. The radial profiles are shown at t = 0 Myr (solid lines), t = 100 Myr (dotted lines) and t = 500 Myr (dashed lines). The number objects belonging to the heavier species is $N_1 = 100$, whereas for the lighter species $N_2 = 15260$. Thus, the total mass in species 1 is much less than the total mass in species 2, and Spitzer's Criterion is satisfied.

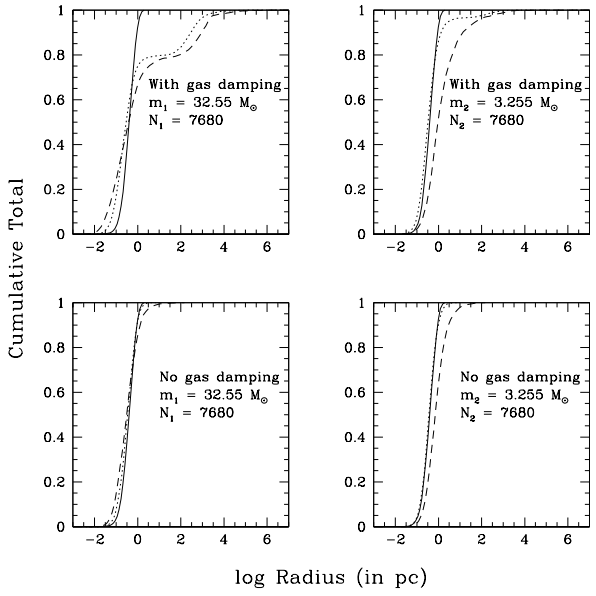

Figure 6. The cumulative radial density profiles are shown for the low- (bottom insets) and high-mass (top insets) species, both with (left insets) and without (right insets) gas damping. The radial profiles are shown at t = 0 Myr (solid lines), t = 100 Myr (dotted lines) and t = 500 Myr (dashed lines). The number of objects belonging to each mass species is equal, with $N_1 = N_2 = 7680$.

mation, young open clusters or associations, and primordial globular clusters.

4.1 Mass segregation and energy equilibrium

Here, we discuss the implications of our results for the rate of mass segregation in a gas-embedded star cluster within the context of energy equilibrium.

Within the framework of our analytic model, if initially all mass species in a cluster have the same root-mean-square speed, then all three damping mechanisms considered in this paper will push this initial state toward energy equilibrium. Our simulations show that energy equipartition is never actually achieved, even without gas damping (see Trenti & van der Marel (2013) for more details). The analytic timescale presented in Appendix A and compared

to the simulations in Figure 3 nonetheless approximately describe the timescale for mass segregation due to gas dynamical friction[5] to within an order of magnitude, since this timescale depends most sensitively on the *initial* particle velocity, with the dependence on the *final* particle velocity typically being negligible.

Our results illustrate that both gas dynamical friction and accretion from the ISM should serve to accelerate the rate of mass segregation (or stratification) within gas-embedded star clusters, operating on timescales comparable to (albeit typically smaller than) the corresponding timescale for two-body relaxation for typical gas densities and cluster masses. Importantly, we do not expect either gas accretion or gas dynamical friction to stop operating once mass segregation is achieved. These mechanisms will continue to reduce the velocities of more massive particles the fastest, causing the cluster to fall further away from energy equilibrium, and contract even further. In particular, clusters that would otherwise achieve a stable state of approximate energy equilibrium will be forced out of this state by gas damping. Thus, so long as gas damping continues to operate, a stable state of energy equilibrium cannot be achieved. Eventually, the central density of the heavier particles becomes sufficiently high that they begin to undergo strong gravitational interactions, progressively dwindling their population size by ejecting each other from the cluster (or colliding).

In massive clusters, gas damping could push clusters to core collapse on a shorter timescale than two-body relaxation alone. This could help to explain why more massive Galactic globular clusters are, on average, more concentrated (Harris 1996, 2010 update; Leigh et al. 2013b), when two-body relaxation alone should cause the opposite. That is, two-body relaxation causes the concentration to increase slowly over time, but this process operates at a rate that is inversely proportional to the cluster mass. For this scenario to be compatible with the observed distribution of concentrations, our analytic results suggest that the duration of the gas-embedded phase should be proportional to the total cluster mass. This is because the additional gas mass increases the stellar velocities via the virial theorem, and the timescale for gas damping to decelerate a massive test particle scales with the cube of the particle velocity in the steady-state supersonic limit. Thus, the duration of the gas-embedded phase should scale with total cluster mass as $M_{clus}^{2/3}$, since $\tau_{gd,sup} \propto \sigma^3$ and $\sigma \propto M_{clus}^{1/2}$. Here, $\tau_{gd,sup}$ represents the timescale for gas damping (i.e. either gas accretion or gas dynamical friction) to operate in the steady-state supersonic limit and σ is the stellar velocity dispersion, taken as a proxy for the typical relative velocity between stars and the gas. If the duration of the gas-embedded phase does indeed scale with the total cluster mass, then this could predict a relation between second generation stars and the concentration parameter, perhaps in the form of a correlation between concentration and the fraction of second generation stars (see Section 4.3.1 below).

Alternatively, assuming that the total mass in stars greatly exceeds the total gas mass (so that the stellar velocities do not depend strongly on the total gas mass, via the virial theorem), then more massive clusters could end up more concentrated if the gas fraction scales linearly with the total cluster mass, and the duration of the gas-embedded phase is independent of cluster mass. This is because the rate of gas damping scales linearly with gas density, and we assume that the cluster half-mass radius r_h is also approximately independent of the total cluster mass (Harris 1996, 2010 update).

Importantly, we expect our main conclusions to hold if our simulations were to be re-performed with a realistic mass spectrum. In particular, gas damping should still accelerate the rate of mass segregation, cause overall cluster contraction and even accelerate the rate of core collapse. However, we caution that higher gas densities than adopted in the simulations performed in this paper will likely be required to achieve comparable effects within a few 100 Myr. This is because the average mass in our simulations is higher than it would be assuming a realistic mass spectrum, increasing the efficiency of gas damping. We did attempt to perform some simulations adopting a realistic mass spectrum, and our preliminary results confirm these conclusions.

4.2 Model assumptions

In this section, we improve upon the connection between our results and real astrophysical environments by discussing our model assumptions.

First, we discuss our derivation for the timescale for two-body relaxation to operate in a gas-embedded star cluster, as presented in Equation A5. Importantly, we have modeled the gas as a simple background potential in this derivation, which neglects the gravitational interactions between stars and over-densities in the gas such as, for example, any filamentary structure in the gas. We do not expect our model to be accurate in the regime where the total gas mass significantly exceeds the total stellar mass, since here the assumption that the cluster is in steady-state breaks down, as does the assumption that the gas can be treated as a simple background potential. More detailed numerical simulations will be needed to identify the parameter space suitable to our simple analytic treatment for a gas-modified relaxation time.

Next, we discuss our simplified treatment of gas dynamical friction and accretion. Probably the most important assumption is that the radial density profile of the gas is uniform, which is certainly not the case in most observed star-forming regions. Among other things, the gas could be more centrally concentrated than the stars due to dissipation, and/or it could exhibit over- and under-densities due to radiation pressure from stars and its own self-gravity. If a region is of sufficiently low density, perturbations traveling through the gas may not be able to propagate through it, and this would decrease the effectiveness of gas dynamical friction. What's more, the orbits of neighboring stars pass directly through the wakes induced by gas dynamical friction. This suggests that the true upper limit for the Coulomb logarithm, incorporated in the derivation for the deceleration due to gas dynamical friction in the supersonic regime, should perhaps be the distance between stars, instead of the cluster half-mass radius. This reduces the rate of de-

[5] More accurately, our analytic timescale corresponds more closely to the *onset* of mass segregation due to gas dynamical friction.

celeration due to gas dynamical friction by a factor $\lesssim 10$. These issues are also not accounted for by our simple estimate for the accretion rate. The Bondi-Hoyle-Lyttleton prescription for accretion represents a strict upper limit, and the true accretion rate could be orders of magnitude lower (e.g. Krumholz, McKee & Klein 2004, 2005a, 2006).

Our model is only suited to the steady-state subsonic and supersonic limits, or $v \ll c_{\rm s}$ and $v \gg c_{\rm s}$, respectively. Thus, the assumptions behind our analytic timescales break down for stellar velocity dispersions on the order of the sound speed. Here, gas dynamical friction is at its most efficient, and could be the dominant damping force acting on the test particle for much lower gas densities than our results suggest.

Given the simplicity of our derivations for the mass segregation times due to gas accretion and gas dynamical friction, we estimate they are correct to within an order of magnitude, at best. In fact, given the (flawed) assumption of a uniform gas density, the derived rates are likely overestimates of the true rates. In general, the conclusion that the gas dynamical friction timescale is shorter than the gas accretion timescale for all but the most bloated objects requires further study using more advanced simulations. Indeed, Lee & Stahler (2011) and Lee & Stahler (2013) recently argued that the deceleration due to accretion cannot be separated from that due to gas dynamical friction, and that the damping force is precisely equal to $\dot{m}$v in both the subsonic and supersonic regimes.

To derive the timescales for gas dynamical friction and accretion to cause a massive test particle to become mass segregated, we assumed that both gas damping and two-body relaxation cause a particle's velocity to vary smoothly from an initial value σ to a final value $\sigma\sqrt{\bar{m}/m_1}$. This is not strictly valid, since particles do not adhere to circular orbits in clusters, so that their velocities will vary over the course of a crossing time. In turn, the deceleration due to both gas dynamical friction and accretion should vary over a crossing time, particularly in the supersonic limit, since here both rates depend on the particle velocity. This issue is addressed directly via our computational N-body models, which put the validity of this assumption to the test. Given the reasonably good agreement (to within an order of magnitude) between our analytic model and the results of our simulations, we conclude that the assumption that a particle's velocity varies smoothly as it decelerates due to gas damping is a decent first-order approximation.

4.3 Specific astrophysical environments

When do the initial conditions adopted in our analytic model actually occur in nature? In particular, our model assumes that initially all mass species have the same root-mean-square speed. This assumption should be suitable to a cluster that has recently undergone a phase of violent relaxation. In open clusters, this could occur if the parent star-forming region is initially sub-virial, and a pronounced infall phase occurs. This could also apply to the formation of nuclear star clusters in galactic nuclei. However, here, violent relaxation could also occur when significant reservoirs of gas fall into the nucleus, or when/if other star clusters, in particular massive globular clusters, spiral in and merge with the nucleus due to stellar dynamical friction within the host galaxy.

In all galactic nuclei and young star-forming regions considered in this paper, the stellar motions should typically be in the supersonic regime, since either the gas is predominantly cold and molecular or the stellar velocity dispersion is very high. Nevertheless, it is possible that in some environments, the gas is sufficiently heated by, for example, stellar winds, supernovae, or high-energy radiation, that the gas sound speed becomes on the order of the stellar velocity dispersion. Indeed, the gas in the Galactic Centre within ~ 1 pc of the SMBH is known to be hot (kT ~ 1 keV) (Merritt 2013), however here the stellar velocity dispersion is also high. We note that, when the stellar velocities are on the order of the sound speed, gas damping should be maximally effective, since the deceleration due to gas dynamical friction becomes very large (e.g. Ostriker 1999).

Below, we discuss in more detail the implications of our results for specific astrophysical environments.

4.3.1 Galactic nuclei and primordial globular clusters

The results of our analytic model suggest that, although the rate of gas damping should increase with increasing gas density, the effect is largely canceled by the additional gas mass causing an increase in the stellar velocity dispersion. This suggests that the total duration of the gas-embedded phase plays a more important role in deciding the overall effects of gas damping on the cluster structure than does the gas density. In late-type galaxies, galactic nuclei are thought to undergo continual gas replenishment from the host galaxy. If a new stellar population is born every time this occurs, a correlation could exist between the number of distinct stellar populations and the overall compactness of the nuclear cluster, assuming that the duration of each gas-embedded phase stays roughly the same between gas replenishment events. Additionally, there is some evidence to suggest that more massive GCs are more likely to host multiple stellar populations (e.g. Gratton, Carretta & Bragaglia 2012). This is in rough agreement with the idea that more compact (or concentrated) clusters should also host a larger fraction of second or even third generation stars, or perhaps just a wider stellar age distribution if distinct generations are not present.

As discussed, gas damping should cause clusters to contract, independent of the mass segregation process. The effect can be significant. For example, in our simulations with gas damping, we find a factor of ~ 2 difference in the final cluster half-mass radius compared to those simulations without gas damping, for our chosen model assumptions.

In galactic nuclei, cluster contraction could be relevant to SMBH formation in the early Universe, and even SMBH growth at later cosmic epochs. If an SMBH is present at the centre of a nuclear star cluster, gas damping will increase the feeding rate of stars into its immediate vicinity, and hence the rate at which stars merge with it. More generally, gas damping could accelerate a phase of runaway mergers to occur in the centres of nuclear clusters, which could then result in SMBH formation or growth. The simulations performed in this paper treat all objects as point particles, so that mergers/collisions are neglected. However, modern simulation-based techniques can address this issue

(e.g. Portegies Zwart et al. 2004), which offers an interesting avenue for future studies. Similarly, our results can be applied to stellar-mass black holes in primordial globular clusters, which suggests that gas damping could have an important bearing on the present-day black hole retention fractions.

We caution that we have not considered stellar evolution-induced mass loss in our simulations, which contributes to cluster expansion. This is particularly important early on in the cluster lifetime, when massive stars are still present (e.g. Chernoff & Weinberg 1990; Leigh et al. 2013b). We have also neglected dynamical interactions involving binary stars, which can act either as a source of heating or cooling (e.g. Fregeau, Ivanova & Rasio 2009; Converse & Stahler 2011; Leigh et al. 2013b). Future more sophisticated simulations should ideally account for these processes, and their implications for the results presented here.

4.3.2 Young open clusters

Most young open clusters are not yet in virial equilibrium, and hence are not in steady-state. In some cases, the clusters are sub-virial, and are in the process of contracting. This is exactly what we would expect if gas dynamical friction and/or accretion are acting. Specifically, the stellar velocities should be lower than expected from the virial theorem given the currently observed cluster size and structure. With gas dynamical friction and accretion operating, the stars should continually be decelerating, while also attempting to adjust the cluster structure accordingly. The former must take place before the latter can occur. Thus, both gas dynamical friction and accretion could contribute to causing a gas-embedded cluster to appear sub-virial.

If star clusters are born primordially mass segregated, our analytic timescales do not strictly apply. Indeed, several recent studies suggest that star-forming regions could be mass segregated as early as the protostellar phase (e.g. Kryukova et al. 2012; Elmegreen, Hurst & Koenig 2014; Kirk, Offner & Redmond 2014). However, with our results in mind, it is perhaps no surprise that many young open clusters appear primordially mass segregated, if this conclusion is based on the ages of the clusters being much shorter than their half-mass relaxation times. All of the mechanisms contributing to mass segregation discussed in this paper should be operating *during* the star formation process, and their rates could be relatively short compared to the star formation time. As protostars accrete mass from the ISM, conservation of momentum should continually act to reduce (typically) the velocities of the protostars. At the same time, protostars are being accelerated/decelerated by the gravitational tug from their peers. The most massive protostars should experience the greatest overall deceleration due to momentum conservation from accretion, and/or experience the least overall acceleration from their less massive peers. Thus, by the time a statistically significant distribution of protostar masses has formed, it stands to reason that a cluster could already appear mass segregated (e.g. Girichidis et al. 2012b). This represents an extreme application of our model, and is better addressed using more sophisticated numerical simulations of star formation. Previous SPH simulations have shown that stars in the central cluster regions tend to accrete the most due to the higher gas densities, and this is primarily responsible for star clusters appearing primordially mass segregated (Bonnell et al. 1997; Bonnell & Davies 1998; Bonnell et al. 2001). However, primordial mass segregation can be complicated if (massive) clusters are initially born with significant substructure and undergo one or more phases of clump-infall. It is perhaps more likely that the initial conditions of our model would at some point be met if such a scenario were to occur (e.g. Maschberger et al. 2010).

If our simulations were to be repeated assuming a more realistic gas density profile that follows that of the stars, many of the effects discussed in this paper would be amplified, such as the acceleration of core collapse. In general, we do not consider the evolving properties of the gas, and could be missing a lot of interesting physics due to this simplifying assumption. Our analytic model is meant to provide a useful benchmark for comparison between observational data and future more sophisticated numerical simulations.

5 SUMMARY

In this paper, we study the effects of gas damping on the evolution of embedded star clusters. Using a simple three-component analytic model, we compare the rates of mass segregation due to two-body relaxation, accretion from the interstellar medium, and gas dynamical friction in both the supersonic and subsonic regimes. Using observational data in the literature, we apply our analytic predictions to two different astrophysical environments, namely galactic nuclei and young open star clusters. The general predictions of our analytic model are confirmed using numerical N-body simulations, modified to include the effects of gas damping.

The effects of gas damping can be significant in some gas-rich nuclei and even some gas-embedded low-mass open clusters, significantly reducing the timescale for mass segregation below that due to two-body relaxation alone. However, two-body relaxation dominates in both environments considered here. In general, our results suggest that gas damping is relatively inefficient in very massive clusters with long relaxation times, even when the gas density is high. This is because the higher gas density translates into a larger cluster mass, and thus larger stellar velocities via the virial theorem.

Gas damping causes overall cluster contraction. If the cluster is mass segregated, the core radius contracts faster than the half-mass radius, increasing the central concentration and accelerating the rate of core collapse. This effect should be further amplified if the gas density follows the stellar density, and is higher in the central cluster regions. A stable state of approximate energy equilibrium cannot be maintained if gas damping is present, even if Spitzer's Criterion is satisfied. This instability drives the continued dynamical decoupling and subsequent ejection (and/or collisions) of the more massive population.

ACKNOWLEDGMENTS

We kindly thank Eric Rosolowsky and Natasha Ivanova for useful discussions, as well as an anonymous referee whose comments helped to significantly improve our manuscript.

REFERENCES

Allison R. J., Goodwin S. P., Parker R. J., Portegies Zwart S. F., de Grijs R., Kouwenhoven M. B. N. 2009, MNRAS, 395, 1449
Allison R. J., Goodwin S. P., Parker R. J., Portegies Zwart S. F., de Grijs R., Kouwenhoven M. B. N. 2009, ApJ, 700, 99
Bate M. R., Bonnell I. A., Bromm W. 2003, MNRAS, 341, 213
Bate M. R. 2009, MNRAS, 392, 590
Bate M. R. 2012, MNRAS, 419, 3115
Binney J., Tremaine S., 1987, Galactic Dynamics (Princeton: Princeton University Press)
Böker T., Lisenfeld U., Schinnerer E. 2003, A&A, 406, 87
Bondi H., Hoyle F. 1944, MNRAS, 104, 273
Bondi H. 1952, MNRAS, 112, 195
Capuzzo-Dolcetta R., Mastrobuono-Battisti A., Maschietti D. 2011, New Astronomy, 16, 284
Bonnell I. A., Bate M. R., Clarke C. J., Pringle J. E. 1997, MNRAS, 285, 201
Bonnell I. A., Davies M. B. 1998, MNRAS, 295, 691
Bonnell I. A., Bate M. R., Clarke C. J., Pringle J. E. 2001, MNRAS, 323, 785
Chernoff D. F., Weinberg M. D. 1990, ApJ, 351, 121
Conroy C., Spergel D. N. 2011, ApJ, 726, 36
Conroy C. 2012, ApJ, 758, 21
Converse J. M., Stahler S. W. 2011, MNRAS, 410, 2787
Davies M. B., Miller M. C., Bellovary J. M. 2011, ApJ, 740, 42
Dokuchaev V. P. 1964, Sovet Astron., 8, 23
Da Rio N., Robberto M., Hillenbrand L. A., Henning T., Stassun K. G. 2012, ApJ, 748, 14
De Marchi G., Paresce F., Pulone L. 2007, ApJ, 656, L65
De Marchi G., Paresce F., Portegies Zwart S. 2010, ApJ, 718, 105
De Marchi G., Panagia N., Sabbi E. 2011, ApJ, 740, 10
Elmegreen B. G., Hurst R., Koenig X. 2014, ApJL, 782, L1
Fregeau J. M., Ivanova N., Rasio F. A. 2009, ApJ, 707, 1533
Gabor J. M., Bournaud F. 2013, MNRAS, 434, 606
Gieles M., Heggie D., Zhao H. 2011, MNRAS,413, 2509
Girichidis P., Federrath C., Banerjee R., Klessen R. S. 2012, MNRAS, 420, 613
Girichidis P., Federrath C., Allison R., Banerjee R., Klessen R. S. 2012, MNRAS, 420, 3264
Gratton R. G., Bonifacio P., Bragaglia A., Carretta E., Castellani V., Centurion M., Chieffi A., Claudi R., Clementini G., D'Antona F., Desidera S., Francois P., Grundahl F., Lucatello S., Molaro P., Pasquini L., Sneden C., Spite F., Straniero O. 2001, A&A, 369, 87
Gratton R., Carretta E., Bragaglia A. 2012, A&ARv, 20, 50
Harris, W. E. 1996, AJ, 112, 1487 (2010 update)
Heggie D. C., Hut P. 2003, The Gravitational Million-Body Problem: A Multidisciplinary Approach to Star Cluster Dynamics (Cambridge: Cambridge University Press)
Henon M. 1960, Annales d'Astrophysique, 23, 668
Henon M. 1969, A&A, 2, 151
Henon M. 1973, Dynamical Structure and Evolution of Dense Stellar Systems, ed. L. Martinet & M. Mayor (Geneva Obs.) Pringle J. E. 2006, MNRAS, 373, L90
Hopkins P. F., Quataert E. 2011, MNRAS, 415, 1027
Hoyle F., Lyttleton R. A. 1939, in Proceedings of the Cambridge Philosophical Society, 35, 405
Kirk H., Myers P. C. 2011, ApJ, 727, 64
Kirk H., Offner S. S. R., Redmond K. J. 2014, MNRAS, accepted
Kormendy J., Ho L. C. 2013, ARA&A, 51, 511
Krumholz M. R., McKee C. F., Klein R. I. 2004, ApJ, 611, 399
Krumholz M. R., McKee C. F., Klein R. I. 2005, ApJ, 618, 757
Krumholz M. R., McKee C. F., Klein R. I. 2005, Nature, 438, 332
Krumholz M. R., McKee C. F., Klein R. I. 2006, ApJ, 638, 369
Krumholz M. R., Klein R. I., McKee C. F. 2011, ApJ, 740, 74
Krumholz M. R. 2011, ApJ, 743, 110
Krumholz M. R., Klein R. I., McKee C. F. 2012, ApJ, 754, 71
Kryukova E., Megeath S. T., Gutermuth R. A., Pipher J., Allen T. S., Allen L. E., Myers P. C., Muzerolle J. 2012, AJ, 144, 31
Lada C. J., Lada E. A. 2003, ARA&A, 41, 57
Launhardt R., Zylka R., Mezger P. G. 2002, A&A, 384, 112
Lee A. T., Stahler S. W. 2011, MNRAS, 416, 3177
Lee A. T., Stahler S. W. 2013, A&A, accepted
Lee A. T., Cunningham A. J., McKee C. F., Klein R. I. 2014, ApJ, 783, 50
Leigh N. W., Böker T., Maccarone T. J., Perets H. B. 2013, MNRAS, 429, 2997
Leigh N. W., Giersz M., Webb J. J., Hypki A., De Marchi G., Kroupa P., Sills A. 2013, MNRAS, 436, 3399
Lynden-Bell D. 1962a, MNRAS, 123, 447
Lynden-Bell D. 1962, MNRAS, 124, 1
Lynden-Bell D. 1962, MNRAS, 124, 95
Maccarone T. J., Zurek D. R. 2012, MNRAS, 423, 2
Marks M., Kroupa P., Baumgardt H. 2008, MNRAS, 386, 2047
Maschberger Th., Clarke C. J., Bonnell I. A., Kroupa P. 2010, MNRAS, 404, 1061
McKee C. F., Ostriker E. C. 2007, ARA&A, 45, 565
Merritt D. 2013, Dynamics and Evolution of Galactic Nuclei (Princeton: Princeton University Press)
Moeckel N., Bonnell I. A. 2009, MNRAS, 396, 1864
Moeckel N., Bonnell I. A. 2009, MNRAS, 400, 657
Moeckel N., Holland C., Clarke C. J., Bonnell I. A. 2012, MNRAS, 425, 450
Odenkirchen M., Grebel E. K., Dehnen W., Rix H.-W., Yanny B., Newberg H. J., Rockosi C. M., Martinez-Delgado D., Brinkmann J., Pier J. R. 2003, AJ, 126, 2385
Offner S. S. R., Hansen C. E., Krumholz M. R. 2009, ApJL, 704, L124
Offner S. S. R., Klein R. I., McKee C. F., Krumholz M. R. 2009, ApJ, 703, 131

Offner S. S. R., McKee C. F. 2011, ApJ, 736, 53
Osborn W. 1971, Observatory, 91, 223
Ostriker E. C. 1999, ApJ, 513, 252
Parker R. J., Meyer M. R. 2012, MNRAS, 427, 637
Parker R. J., Wright N. J., Goodwin S. P., Meyer M. R. 2014, MNRAS, 438, 620
Perets H. B., Hopman C., Alexander T. 2007, ApJ, 656, 709
Phan-Bao N., Lee C.-F., Ho P. T. P., Tang Y.-W. 2011, ApJ, 735, 14
Piotto G., Bedin L. R., Anderson J., King I. R., Cassisi S., Milone A. P., Villanova S., Pietrin- ferni A., Renzini A. 2007, ApJ, 661, L53
Portegies Zwart S. F., Baumgardt H., Hut P., Makino J., McMillan S. L. W. 2004, Nature, 428, 724
Rephaeli Y., Salpeter E. E. 1980, ApJ, 240, 20
Ruderman M. A., Spiegel E. A. 1971, ApJ, 165, 1
Ruffert M. 1997, A&A, 317, 793
Schinnerer E., Böker T., Meier D. S. 2003, ApJ, 591, L115
Schinnerer E., Böker T., Emsellem E., Lisenfeld U. 2006, AJ, 649, 181
Spitzer L. Jr. 1969, ApJ, 158, 139
Spitzer L. Jr. 1987, Dynamical Evolution of Globular Clusters (Princeton, NJ: Princeton Univ. Press)
Strader J., Chomiuk L., Maccarone T. J., Miller-Jones J. C. A., Seth A. C. 2012, Nature, 490, 71
Tremaine S. D., Ostriker J. P., Spitzer L. Jr. 1975, ApJ, 196, 407
Trenti M., van der Marel R. 2013, MNRAS, doi: 10.1093/mnras/stt1521
Vishniac E. T. 1978, ApJ, 223, 986
von Hippel T., Sarajedini A. 1998, AJ, 116, 1789
Wang W., Boudreault S., Goldman B., Henning T., Caballero J. A., Bailer-Jones C. A. L. 2011, A&A, 531, 164

APPENDIX A: ANALYTIC MODEL

Consider a three-component model for a spherical gas-embedded self-gravitating system of massive particles. The individual masses of the components are m_1, m_2 and m_3, and satisfy the relations $m_1 > m_2 \gg m_3$ and $M_1 \ll M_2 \approx M_3$. Here we let M_1, M_2 and M_3 represent the total masses in components 1, 2 and 3, respectively. Spitzer's Criterion (Spitzer 1969) is satisfied for all permutations of species 1, 2 and 3. Thus, although not guaranteed,[6] energy equipartition, or more accurately energy equilibrium, is in principle possible for our three-component system. As discussed in Section A, energy equipartition typically does not occur in real star clusters and a stable state of energy *equilibrium* tends to be achieved instead (e.g. Trenti & van der Marel 2013). However, as we will show, the precise final velocity does not significantly influence our calculations for the different mass segregation timescales. Thus, we assume a final state of approximate energy equipartition throughout our calculations for simplicity.

[6] Whether or not a self-gravitating system of stars actually achieves energy equipartition is a complicated technical issue (see Trenti & van der Marel (2013) for more details). Spitzer's Criterion merely provides an approximate guide.

Putting our model within the context of a real star cluster, components 1 and 2 constitute the total stellar mass $M_s = M_1 + M_2$, and component 3 constitutes the total gas mass $M_g = M_3$. Instead of the average stellar mass, we use the *root-mean-square* mass in species 1 and 2, denoted by $\bar{m}$ (Perets, Hopman & Alexander 2007). The root-mean-square mass is given by:

$$\bar{m} = \sqrt{\frac{N_1 m_1^2 + N_2 m_2^2}{N_1 + N_2}} \tag{A1}$$

where $N_1 = M_1/m_1$ and $N_2 = M_2/m_2$ denote the number of objects belonging to species 1 and 2, respectively.

Now, consider a test particle of mass m_1 orbiting within the system. Initially, the velocity of the test particle v_1 is set equal to the root-mean-square speed of the system (Spitzer 1969; Binney & Tremaine 1987):

$$\sigma = \sqrt{\frac{2G(M_s + M_g)}{5r_h}}, \tag{A2}$$

where r_h is the half-mass radius of the cluster. In the subsequent sections, we will calculate the timescales for all three damping mechanisms to reduce the speed of the test particle from σ to $\sigma\sqrt{\bar{m}/m_1}$, which signifies energy equipartition and, as discussed in the subsequent section, mass segregation.

A1 Two-body relaxation in gas

In this section, we calculate the rate for gravitational interactions between stars to bring a massive test particle orbiting within a gas-embedded system to an orbit that is roughly consistent with energy equilibrium. We refer to this final state as "mass segregated". We ignore short-range interactions between stars, such as energetic scattering events and direct collisions, since these do not become important until *after* mass segregation has occurred, and the heaviest particles are confined to the bottom of the total cluster potential. We focus only on long-range interactions, specifically modifying the rate of two-body relaxation in a gaseous medium, modeled as a background potential.[7] Here, the terms short- and long-range refer to distances on the order of the stellar and cluster (i.e. half-mass) radii, respectively.

We wish to calculate the time required for the test particle to be decelerated to a mean speed $\sqrt{\bar{m}/m}\sigma$ due to star-star gravitational interactions only. In the absence of gas, this time corresponds to the equipartition time, which is roughly equal to the relaxation time (e.g. Heggie & Hut 2003). For the test particle, this time is given by (Vishniac 1978):

$$\tau_{rh}(m_1) = \frac{\bar{m}}{m_1}\tau_{rh}, \tag{A3}$$

where

$$\tau_{rh}[yr] = 1.7 \times 10^5 N_s^{1/2} \Big(\frac{r_h}{1\mathrm{pc}}\Big)^{3/2} \Big(\frac{1M_\odot}{\bar{m}}\Big)^{1/2}, \tag{A4}$$

[7] The assumption that the gas can be modeled as a simple background potential is likely not valid over the entire range of cluster masses considered here. To first order, we expect it to breakdown when the total stellar mass is much smaller than the total gas mass, or $M_s \ll M_g$. We will return to this issue in Section 4.

and $N_s = N_1 + N_2$ is the total number of stars.

Is this approximation still valid in the presence of gas? We will argue that, if the *shape* of the total gravitational potential is approximately the same with or without the gas, then the rate at which two-body relaxation operates on the stellar mass is the same to within a dimensionless constant, which is equal to the ratio between the total mass in gas and stars. In this approximation, the gas is treated as a simple background potential.

Consider a gravitational potential Φ_s that describes an unrelaxed, self gravitating, steady-state (i.e. virialized) stellar system, based on the corresponding solution to Jeans' equation (see Lynden-Bell (1962b) for examples of such potentials). If we include a gas component with potential $\Phi_g = \alpha\Phi_s$ where $\alpha > 0$, then $\Phi_g + \Phi_s$ is also a solution to Jeans' equation, and describes a steady-state, unrelaxed system.[8]

From Poisson's equation, we have $M_g = \alpha M_s$ for the relation between the total mass in gas and stars.[9] Thus, with these assumptions, we can replace the total mass in stars $M_s = N\bar{m}$ in Equation A4 with $(1+\alpha)M_s$. This gives:

$$\tau_{\rm rh}[yr] = 1.7 \times 10^5 (1+\alpha)^{1/2} N_s^{1/2} \Big(\frac{r_{\rm h}}{1{\rm pc}}\Big)^{3/2} \Big(\frac{1M_\odot}{\bar{m}}\Big)^{1/2}, \quad \text{(A5)}$$

where α is the ratio between the total mass in gas and stars, or $\alpha = M_g/M_s$. This form for the half-mass relaxation time should be reasonable late in the star formation process, after a significant fraction of the gas mass has been converted to stars.

A2 Accretion from the ISM

In this section, we consider how predominantly short-range (i.e. comparable to the stellar radius) gravitational interactions between stars and gas contribute to accelerating the rate of mass segregation above the effects of two-body relaxation (i.e. long-range star-star interactions) alone. To this end, we consider two additional damping mechanisms that could operate on a test particle of mass m.[10] These are gas dynamical friction and accretion from the ISM.

We consider gas dynamical friction and gas accretion as being entirely independent mechanisms. The drag induced by accretion corresponds to the momentum imparted to the accretor from the accreting gas, so that the gas is co-moving with the accretor and gravitationally bound to it. The drag induced by gas dynamical friction, on the other hand, arises due to an asymmetry in the gas flow along the axis of motion of the perturber. Typically, a wake is formed downstream of the perturbing object which exerts a gravitational tug on it, thereby reducing its speed. As we will show, in each of the subsonic and supersonic regimes, the derived timescales for accretion and gas dynamical friction are equivalent to within a dimensionless constant, for a given test particle mass. This is because both timescales are derived assuming spherically symmetric perturbations on the gas, with the degree of damping arising due to the asymmetry induced by the motion of the perturbing object relative to the gas. With that said, we note that Lee & Stahler (2011) recently showed that the rate of momentum damping due to gas dynamical friction is precisely equal to $\dot{m}$v, and that accretion and gas dynamical friction cannot be separated with their formalism into separate damping mechanisms. Regardless, the derived estimates for the rate of deceleration of a particle due to gas dynamical friction by Lee & Stahler (2013) agree well with those of Ostriker (1999) and previous authors in the steady-state supersonic limit.

A2.1 The subsonic limit

The time required for accretion to decelerate the particle by roughly the same amount as is done by two-body relaxation in a single relaxation time was derived in Leigh et al. (2013a) for the subsonic limit. For an accretion rate:

$$\dot{m} = \lambda\delta m^\epsilon, \quad \text{(A6)}$$

this timescale is given by:

$$\tau_{\rm acc} = \frac{m^{1-\epsilon}\Big((m/\bar{m})^{(1-\epsilon)/2} - 1\Big)}{\delta(1-\epsilon)}, \quad \text{(A7)}$$

where $\epsilon > 1$, and λ and δ are coefficients that determine the accretion rate. We set $\lambda = 1.0$ for the remainder of this paper, and absorb this factor into the coefficient δ. For Bondi-Hoyle accretion, $\epsilon = 2$ and we then have for the coefficient (e.g. Bondi & Hoyle 1944; Maccarone & Zurek 2012):

$$\delta = 7 \times 10^{-8} {M_\odot}^{-1} {\rm yr}^{-1} \Big(\frac{n}{10^6{\rm cm}^{-3}}\Big)\Big(\frac{\sqrt{c_s^2+v^2}}{10^6{\rm cms}^{-1}}\Big)^{-3}, \quad \text{(A8)}$$

where n is the particle number density, c_s is the gas sound speed, and v is the velocity of the accretor relative to the gas. Plugging $\epsilon = 2$ into Equation A7 gives:

$$\tau_{\rm acc}[yr] = 1.4{\times}10^8 \Big(1{-}\frac{\bar{m}}{m}\Big)^{-1/2}\Big(\frac{10^6 cm^{-3}}{n}\Big)\Big(\frac{\sqrt{c_s^2+v^2}}{10^6{\rm cms}^{-1}}\Big)^3\Big(\frac{1M_\odot}{m}\Big). \quad \text{(A9)}$$

Importantly, Equation A9 is only valid in the subsonic regime when $v \lesssim c_s$, since it assumes that the velocity of the accretor relative to the gas remains roughly constant as it accretes. Thus, it corresponds to an upper limit, since accretion serves to reduce the accretor's speed, which in turn accelerates the rate of accretion. In the limit $v \ll c_s$, we can modify Equation A9 by dropping the velocity term:

$$\tau_{\rm acc,sub}[yr] = 1.4{\times}10^8 \Big(1{-}\frac{\bar{m}}{m}\Big)^{-1/2}\Big(\frac{10^6 cm^{-3}}{n}\Big)\Big(\frac{c_s}{10^6{\rm cms}^{-1}}\Big)^3\Big(\frac{1M_\odot}{m}\Big). \quad \text{(A10)}$$

A2.2 The supersonic limit

If the motion is in the supersonic regime, i.e. $v \gtrsim c_s$, then changes in the accretor velocity can have an important bearing on the accretion rate. Hence, in this case, we must also integrate over the relative velocity between the gas and the accretor. In Leigh et al. (2013a), this was not necessary, since we considered only a single (high) value for the sound

[8] This is only valid in the supersonic regime, where pressure forces are negligible in the gas and the collisionless Boltzmann equation applies. In the subsonic regime, we simply assume that steady-state is achieved.

[9] Note that we do not specify a functional form for the radial density profile, and will work with the average cluster gas density from here on out.

[10] Throughout this section, we replace m_1 by the more general variable m, since the derived timescales apply to any massive celestial object.

speed, and the motion was not supersonic. In this paper, however, we are interested in a range of sound speeds, and must deal with supersonic motion. Thus, we must re-derive Equation A9 to obtain an analogous expression in the supersonic regime for the approximate time required for the test particle to become mass segregated. We assume $v \gg c_{\rm s}$ throughout this derivation in order to ensure a consistent comparison to the corresponding timescale for gas dynamical friction, derived in the subsequent section.[11]

We write:

$$\tau_{acc} = \int_{m}^{\sqrt{m^3/\bar{m}}} \frac{dm}{\dot{m}}. \tag{A11}$$

We can take $\delta \propto v^{-3}$ in Equation A8 for the supersonic regime, since we assume $v \gg c_{\rm s}$. Hence, plugging Equations A8 and A6 into Equation A11 and using conservation of momentum, we obtain for the time needed for accretion to reduce the test particle's speed from σ to $\sqrt{m/\bar{m}}\sigma$ in the supersonic regime:

$$\tau_{\rm acc,sup}[yr] = 3.5{\times}10^7\Big(1{-}\Big(\frac{\bar{m}}{m}\Big)^2\Big)\Big(\frac{10^6{\rm cm}^{-3}}{n}\Big)\Big(\frac{v}{10^6{\rm cms}^{-1}}\Big)^3\Big(\frac{1M_\odot}{m}\Big). \tag{A12}$$

A2.3 Direct accretion

In the limit where the test particle velocity exceeds the escape speed from its surface, Bondi-Hoyle-Lyttleton accretion no longer applies. This is because the radius of the object becomes larger than the gravitationally-focused cross-section. Thus, in this regime, it is the direct plowing of the gas by the test particle that reduces its momentum, and hence speed. We refer to this as *direct accretion*. This scenario is the most relevant to low-mass, bloated objects orbiting in an environment with a high velocity dispersion. The timescale required for direct accretion to bring a test particle into approximate energy equipartition can be calculated as the time required for an object of cross-sectional area πR^2 to collide with sufficient gas mass to reduce its speed from σ to $\sqrt{m/\bar{m}}\sigma$ using conservation of momentum. Using this approximation, we calculate a timescale on the order of 100 Myr for an object with m $\sim$ 1 $M_\odot$ and R $\sim$ 1000 $R_\odot$, which is applicable to a star in the asymptotic giant branch (AGB) phase of evolution. This is shorter than the corresponding timescale for gas dynamical friction, but longer than the typical duration of the AGB phase. Assuming instead R $\sim$ 100 $R_\odot$, this timescale is on the order of a Hubble time. Thus, we do not expect direct accretion to dominate the deceleration of any test particle over the majority of its lifetime. Importantly, our derivation ignores AGB winds and radiation, and how these interact with the surrounding ISM prior to direct accretion, which could increase $\tau_{\rm acc,dir}$ substantially. Thus, for these reasons, we do not concern ourselves with the direct accretion scenario in the subsequent sections.

[11] We do not address the case $v \sim c_{\rm s}$ analytically, since the assumptions adopted for the subsonic and supersonic regimes do not apply here, and the complexity of the problem increases greatly.

A3 Gas dynamical friction

To derive the time required for gas dynamical friction to decelerate the test particle from σ to $\sqrt{\bar{m}/m}\sigma$, we use the gas dynamical friction force taken from Ostriker (1999):

$$F_{\rm df} = ma_{\rm df} = -F_0 I, \tag{A13}$$

where I is a function that depends on the ratio between the perturber velocity and the gas sound speed $c_{\rm s}$, which changes depending on whether the motion is subsonic or supersonic, and:

$$F_0 = \frac{4\pi(Gm)^2\rho_{\rm g}}{v^2}, \tag{A14}$$

where v is again the velocity of the perturber relative to the gas, and $\rho_{\rm g}$ is the gas density.

Using Equation A13 for the deceleration, we have for the total time:

$$\tau_{\rm df} = \int_{v_{\rm i}}^{v_{\rm f}} \frac{dv}{a_{\rm df}}. \tag{A15}$$

where $v_{\rm i} = \sigma$ and $v_{\rm f} = \sqrt{\bar{m}/m}\sigma$. We must integrate over the test particle velocity since the deceleration induced by the gas dynamical friction force is a function of v. We note that we assume that the particle mass remains constant throughout this calculation, since we are treating accretion and gas dynamical friction independently.

The function I depends on the velocity of the test particle relative to the sound speed, called the Mach number, and takes on two different forms depending on whether the motion is subsonic or supersonic. In the subsonic regime, i.e. $v < c_{\rm s}$, we have (Ostriker 1999):

$$I_{\rm sub} = \frac{1}{2}\ln\frac{c_{\rm s}+v}{c_{\rm s}-v} - v/c_{\rm s}. \tag{A16}$$

In the supersonic regime, i.e. $v > c_{\rm s}$, we have:

$$I_{\rm sup} = \frac{1}{2}\ln\Big(1-\frac{c_{\rm s}^2}{v^2}\Big) + \ln\Big(\frac{r_{\rm max}}{r_{\rm min}}\Big), \tag{A17}$$

where the last term corresponds to the Coulomb logarithm. We take $r_{\rm max} = r_{\rm h}$ and $r_{\rm min} = R$, where R is the physical radius of the test particle. Note that for large radii R, the Coulomb logarithm is smaller and so is the corresponding gas dynamical friction timescale.

A3.1 The subsonic limit

First, we solve for the time needed for the speed of the test particle to be reduced to $\sqrt{\bar{m}/m}\sigma$ in the subsonic limit. To do this for any velocity, we must plug Equation A16 into Equation A15 and integrate with respect to v. The integration must be performed numerically if $v \lesssim c_{\rm s}$, and provides the desired timescale for gas dynamical friction in the subsonic regime, as a function of the gas density and root-mean-square speed of the stellar system. If gas dynamical friction is highly subsonic, i.e. $v \ll c_{\rm s}$, then $I_{\rm sub}$ approaches $(v/c_{\rm s})^3/3$, and the drag force is proportional to the perturber's velocity. Thus, in the limit of a very slow perturber, a simple analytic timescale for gas dynamical friction can be derived:

$$\tau_{\rm df,sub}[yr] = 2.6{\times}10^8\Big(\ln\Big(\frac{m}{\bar{m}}\Big)\Big)^{-1}\Big(\frac{10^6 cm^{-3}}{n}\Big)\Big(\frac{c_{\rm s}}{10^6 cm/s}\Big)^3\Big(\frac{1M_\odot}{m}\Big). \tag{A18}$$

A3.2 The supersonic limit

To obtain the timescale for gas dynamical friction in the supersonic limit, or $\tau_{\rm df,sup}$, the procedure is exactly analogous as in the subsonic regime, except that it is Equation A17 that is plugged into Equation A15. Again, the integration must be performed numerically if $v \gtrsim c_{\rm s}$. However, as the motion becomes highly supersonic, i.e. $v \gg c_{\rm s}$, then $I_{\rm sup}$ approaches $\ln r_{\rm max}/r_{\rm min}$ and the drag force is proportional to v^{-2}. Thus, in the limit of a very fast perturber, the timescale for gas dynamical friction becomes:

$$\tau_{\rm df,sup}[yr] = 2.9{\times}10^{6}\Big(1{-}\Big(\frac{\bar{m}}{m}\Big)^{3/2}\Big)\Big(\frac{10^{6}cm^{-3}}{n}\Big)\Big(\frac{v}{10^{6}cm/s}\Big)^{3}\Big(\frac{1M_{\odot}}{m}\Big), \tag{A19}$$

where here we have used $\ln r_{\rm max}/r_{\rm min} = 10$ for the Coulomb logarithm.

This paper has been typeset from a TEX/ LATEX file prepared by the author.